STEM CELLS AND DEVELOPMENT
Volume 23, Number 23, 2014

DOI: 10.1089/scd.2014.0231

Fast-Proliferating Adipose Tissue Mesenchymal-Stromal-Like Cells for Therapy

Elisabet Aguilar,[1] Julio Rodriguez Bagó,[2] Carol Soler-Botija,[3] Maria Alieva,[4] Maria Angeles Rigola,[5] Carme Fuster,[5] Olaia F. Vila,[6,7] Nuria Rubio,[6,7] and Jeronimo Blanco[6,7]

Human mesenchymal stromal cells, whether from the bone marrow or adipose tissue (hASCs), are promising cell therapy agents. However, generation of abundant cells for therapy remains to be a challenge, due to the need of lengthy expansion and the risk of accumulating genomic defects during the process. We show that hASCs can be easily induced to a reversible fast-proliferating phenotype (FP-ASCs) that allows rapid generation of a clinically useful quantity of cells in <2 weeks of culture. Expanded FP-ASCs retain their finite expansion capacity and pluripotent properties. Despite the high proliferation rate, FP-ASCs show genomic stability by array-comparative genomic hybridization, and did not generate tumors when implanted for a long time in an SCID mouse model. Comparative analysis of gene expression patterns revealed a set of genes that can be used to characterize FP-ASCs and distinguish them from hASCs. As potential candidate therapeutic agents, FP-ASCs displayed high vasculogenic capacity in Matrigel assays. Moreover, application of hASCs and FP-ASCs in a fibrin scaffold over a myocardium infarct model in SCID mice showed that both cell types can differentiate to endothelial and myocardium lineages, although FP-ASCs were more potent angiogenesis inducers than hASCs, at promoting myocardium revascularization.

Introduction

Mesenchymal stromal cells (MSCs) are an auspicious source of multipotent adult stem cells for therapy. Compared with other stem cell sources, such as embryonic or tissue-specific stem cells, MSCs have many advantages, among which ease of isolation, ethical acceptance, low immunogenicity, possible autologous application, reasonable oncological safety, and, in particular, their capacity to home to injured tissues are most desirable. A growing number of publications indicate that MSCs secret a variety of growth factors and chemokines with paracrine effects, which could be responsible of modulating the local environment and/or activating endogenous progenitor cells. Some authors show evidence that points to adipose-derived MSCs as vascular stem cells [1,2].

Historically, bone marrow MSCs were one of the first cell types used for therapy, and are still now the most frequently investigated for such purpose. More recently, however, use of human adipose-tissue-derived MSCs (hASCs) has gained wide acceptance in regenerative clinical applications [3]. Besides their recognized similarity with bone marrow MSCs [4,5], being more abundant, proliferative, and easy to isolate with relatively little trauma and pain make hASCs the choice candidate for some cell therapy applications. Evidence from extensive research and clinical trials supports the therapeutic use of hASCs for a wide range of conditions, including myocardial infarcts, diabetes, or different types of neurological disorders, among others [6–8]. However, if cell therapy has to fulfill its promise as a medicine of the future, then there are still important challenges to overcome. One of the main obstacles for therapy is the generation of large quantities of cells, in a reasonable time period. Thus, despite the availability of large numbers of hASCs from adipose tissue, in vitro expansion is still required to obtain therapeutically effective quantities, of the order of 1–5 million

[1]Human DNA Variability Department, GENYO—Centre for Genomic and Oncological Research (Pfizer/University of Granada/Andalusian Regional Government), PTS Granada, Granada, Spain.
[2]Division of Molecular Pharmaceutics, UNC Eshelman School of Pharmacy, Biomedical Research Imaging Center, University of North Carolina, Chapel Hill, North Carolina.
[3]ICREC Research Program, Fundació Institut d'Investigació en Ciències de la Salut Germans Trias i Pujol (IGTP), Badalona, Spain.
[4]Hubrecht Institute-KNAW and University Medical Centre Utrecht, Utrecht, The Netherlands.
[5]Unit of Cellular Biology and Medical Genetics, Department of Cellular Biology, Physiology and Immunology, Faculty of Medicine, Universitat Autònoma de Barcelona, Barcelona, Spain.
[6]Cell Therapy Group, Institute for Advanced Chemistry of Catalonia (IQAC), CSIC, Barcelona, Spain.
[7]Networking Biomedical Research Center on Bioengineering, Biomaterials and Nanomedicine (CIBER-BBN), Barcelona, Spain.

MSCs per kg body weight, and in some cases, multiple inoculations are needed. The time required to produce such cell quantities is an inverse function of doubling time, which can oscillate between 2 and 6 days [9], and is closely linked to the age of the culture and growth conditions. In standard culture conditions, up to ~75 days may be required to generate 10^{10} hASCs, a prohibitive delay for some applications and, in several clinical trials, it was not possible to obtain quantities of 10^8 cells within a 4-week period [10,11]. In addition, ex vivo expansion capacity is limited and it decreases over time; thus, optimization of culture conditions for large-scale production of safe and functional hASCs is crucial for therapeutic applications.

Numerous laboratories have focused their efforts toward this objective and performed extensive searches on this optimization. For translation into the clinic, hASCs require the use of defined serum-free and xeno-free media (SF/XF) to prevent undesirable immune reactions and contamination by exogenous pathogens [12]. Miettinen and coworkers [13] have also described a totally SF/SX media for hASCs that while preserving differentiation potential and expression of the majority of cell markers, with the exception of CD54, induces faster cell proliferation, a convenient property for clinical applications. Search for growth-promoting additives is another important area in the field of hASC culture and expansion [14–18]. However, analysis of contribution of individual growth factors and other components in defined medium has proven difficult due to synergistic effects resulting from their interactions when used in combination [19–24]. The use of specific media such as EGM-2 has allowed groups like Marchal et al. [25] describe the purification from hASC populations of an endothelial-like cell type with potential application for myocardium repair. This is a key issue in most clinical applications since establishment of a vascular system is essential for tissue repair.

In the current work, we describe a simple method to achieve clinically useful cell numbers. We show that hASCs acquire a fast-proliferating phenotype (FP-ASCs) when grown in EGM-2 (Cambrex) medium that allows the generation of up to 10^{10} cells in a 20-day growth period, starting from a single culture of 5×10^5 cells and without sacrificing their functional properties or safety. We also show a procedure for their characterization and compare their therapeutic capacity with that of hASCs in an acute myocardium infarct mouse model.

Materials and Methods

Cell culture

hASCs were isolated from adipose tissue derived from cosmetic subdermal liposuctions, as described previously [26]. Liposuction samples were obtained from Dr. Josep Roca, after informed written consent from anonymous donors from ''System-Roca'' (Centro Medico Delfos). Work with human samples was approved by the Bioethical Subcommittee of Superior Council of Scientific Research. We evaluated cells from four donors: patient 1: 44-year old, female, body mass index (BMI) 28, 35; patient 2: 51-year old, female, BMI 29, 59; patient 3: 49-year old, female, BMI 27, 47; and patient 4: 46-year old, female, BMI 29, 15. Briefly, lipoaspirate was suspended in 1X collagenase type I (Invitrogen) solution and incubated at 37°C and inactivated by addition of Dulbecco's modified Eagle's medium-high glucose (DMEM-hg) + 10% fetal bovine serum (FBS). hASCs were isolated by plastic adherence. Cells were seeded at a density of 3,000 cells/cm^2 and grown in two different media: in DMEM-hg, 10% heat-inactivated FBS (Sigma), 2 mM L-glutamine (Sigma), and 50 U/mL penicillin/streptomycin (Sigma) to grow hASCs in standard conditions and, in EGM™-2 Bullet-kit™ (Lonza), 10% heat-inactivated FBS (Sigma) and plates precoated with fibronectin (BD Biosciences) [10 μg/mL in phosphate-buffered saline (PBS)] to culture FP-ASCs.

Phenotypic analysis by flow cytometry

hASCs were trypsinized, washed, and resuspended in PBS with 1% bovine serum albumin (Sigma). Cells were incubated in the dark at room temperature for 1 h with the following monoclonal antibodies conjugated with phycoerythrin: CD49d, CD54, CD106, CD73, CD90, CD144, CD13, CD44, CD29 (BD Biosciences), CD31, C-Kit, CD34, CD105 (Abcam), VEGFR (R&D Systems), and CD133 (Milteny). Unspecific binding was assessed by isotype control mouse IgG2α-PE and mouse IgG1κ-PE (BD Bioscience). Cells were then washed in PBS and analyzed by FACS in an EPICS XL™ Flow Cytometer.

Differentiation assays

For in vitro adipogenic and osteogenic differentiation, cells were cultured in StemPro Adipogenesis and Osteogenesis Differentiation Kit, respectively (Gibco), during a 14-day period, following the manufacturer's instructions.

Measurement of doubling time and total cell number

The average doubling time of cells was calculated during the logarithmic growth phases, according to the following formula: doubling time = time (days)/$\log_2$ (N_2/N_1), where N_1 is the first cell count and N_2 is the cell count at the end of logarithmic growth phases. The total cell number after the initiation of culture was also measured by seeding the cells at a density of 3,000 cells/cm^2 and culturing the cells until they reached the stationary phase.

Determination of cell senescence

The senescent state of the cells was determined using the Senescence Cell Histochemical Staining Kit (Sigma). Both cell types were stained in logarithmic and stationary growth phases following the manufacturer's instructions, incubating at 37°C without CO_2 overnight.

Determination of tumorigenic capacity in vivo by noninvasive bioluminescence imaging

Cells, 5×10^5, labeled with pRRL-PLuc-IRES-EGFP [27] were inoculated intramuscularly in each thigh muscle. Adult 6-week-old SCID mice were purchased from Charles River Laboratories and kept under pathogen-free conditions in laminar flow boxes. Animal maintenance and experiments were performed in accordance with established guidelines from the Catalonian Government and protocol approved by Direcció General del Medi Natural, Generalitat de Catalunya. For in vivo bioluminescence imaging (BLI) of *Photinus*

pyralis luciferase (PLuc) activity, anesthetized mice were intraperitoneally injected with 150 μL of luciferin (16.7 mg/mL in physiological serum; Caliper). The cells were followed by noninvasive BLI during 160 days, using a high-efficiency ORCA-2BT Imaging System (Hamamatsu Photonics). Analysis of images was performed using the Wasabi software (Hamamatsu Photonics).

Comparative genomic hybridization analysis

DNA was extracted from cells using FlexiGene DNA kit (Qiagen), following the manufacturer's instructions. Comparative genomic hybridization (CGH) analysis was performed as described previously [28]. DNA for tests (hASCs and FP-ASCs) was labeled with Spectrum Red–dUTP, whereas reference DNA was labeled with Spectrum Green–dUTP by nick translation using a commercial kit (Vysis). After hybridization, the slides were washed according to manufacturer's instructions and were mounted in Vectashield (Vector Laboratories) containing 4,6-diamidino-2-phenylindole, resulting in a G band-like pattern that was used for chromosome identification. An average of 10 metaphases per hybridization were analyzed using the Metasystems Isis V5.C software (Metasystems). The average red:green fluorescent ratio for each chromosome was determined by the CGH software. Deviations of the ratio <0.75 (the test DNA is under-represented) or >1.25 (the test DNA is over-represented) were scored as loss or gain of material in the test sample, respectively.

Microarrays

Total RNA was extracted from cells, using the RNAeasy mini kit (Qiagen) according to the manufacturer's instructions. Microarrays were processed at Functional Genomics Core of Institute for Research in Biomedicine. Briefly, 25 ng of total RNA was amplified using the TransPlex® Complete Whole Transcriptome Amplification kit (Sigma) and subsequently labeled using GeneChip Mapping 10K Xba Assay kit (Affymetrix), according to manufacturer's instructions. Affymetrix GeneChip Human Gene 1.0ST arrays were hybridized with 8 μg of labeled, amplified dsDNA; washed; stained; and scanned according to the protocol described in Affymetrix GeneChip® Expression Analysis Manual (fluidics protocol FS450_007). Scanning was done on an Affymetrix GeneChip Scanner 7G. Normalized expression signals were calculated from Affymetrix CEL files using RMA [29]. Affymetrix results were interpreted with the Partek Genomics Suite (Partec, Inc.). *P*-values were corrected using a step-up false discovery rate of 20% and the resulting list was filtered to include only genes that demonstrated 1.5-fold, or larger, up- or down-regulation in FP-ASCs relative to hASCs. We performed an Ingenuity Knowledge Base search using the Ingenuity Pathway Analysis (IPA) application to obtain a biological analysis.

Real-time polymerase chain reaction

Two micrograms of total RNA used in microarrays was reverse transcribed using the Revertaid First Strand cDNA Synthesis kit (Fermentas). cDNA was real-time polymerase chain reaction (RT-PCR) amplified, using the ABI PRISM 7000® (Applied Biosystems). FAM-labeled primer/probes were purchased from Applied Biosystems: CNR1 (Hs01038522_s1), EFNB2 (Hs00187950_m1), FKBP5 (Hs01561006_m1), HSD 11B1 (Hs01547870_m1), PTEGR2 (Hs00168754_m1), HGF (Hs00300159_m1), AREG/AREGB,CPM (Hs01074151_m1), MAOA (Hs00165140_m1), ZBTB16 (Hs00957433_m1), ALOX15B (Hs00153988_m1), CCL20 (Hs01011368_m1), and GAPDH (Hs99999905_m1). Data were collected and analyzed on the ABI Prism 7000 Sequence Detection System (ABI). Each sample was analyzed in duplicate. The Δ threshold cycle (Ct) method was used to quantify relative expression for each gene using GAPDH as endogenous reference.

Lentiviral particle production and cell transduction

Lentiviral production was done as described previously [30]. Four lentiviral vector constructs were used to label cells. For tumorigenic assay, cells were transduced using pRRL-PLuc-IRES-EGFP-concentrated lentiviral stock (Multiplicity of Infection [MOI] = 21) during 48 h; vector was a kind donation from L. Alvarez-Vallina [27]. To monitor in vivo differentiation, cells were transduced using CMV:hRLuc:RFP:ttk-concentrated lentiviral stock (MOI = 21) during 48 h. The highest 11% RFP-expressing cells were selected by FACS. Sorted cells were transduced again with either concentrated lentiviral Plox:hPECAM-1p:PLuc:EGFP or Plox:hcTnIp:PLuc:EGFP stock (MOI = 21) during 48 h to obtain double-transduced cells: hPECAM-1p:PLuc:EGFP/CMV:RLuc:RFP:ttk cells and hcTnIp:PLuc·EGFP/CMV:RLuc:RFP:ttk-cells, respectively. CMV:hRLuc:RFP:ttk vector was a kind gift from S.S. Gambhir (Dept. of Radiology, Stanford University), Plox:hPECAM-1p:PLuc:EGFP and Plox:hcTnIp:PLuc:EGFP vectors were constructed in our group [31].

Myocardial infarction model

The study was performed on 24 female SCID mice (15-weeks old, 20–25 g; Charles River Laboratories). Animal maintenance and experiments were performed in accordance with established guidelines from the Catalonian Government and protocol approved by Direcció General del Medi Natural, Generalitat de Catalunya. Myocardial infarction was created as previously described [32]. Briefly, the animals were intubated and anesthetized with a mixture of O^2/isoflurane and mechanically ventilated. The heart was exposed and the left anterior descending coronary artery was permanently occluded with an intramural stitch (7-0 silk suture). Mice were then randomly distributed into four experimental groups: control miocardial infarction (MI), control MI with fibrin patch implantation, and MI with implantation of cell-loaded fibrin patch (hASCs or FP-ASCs).

Development and delivery of fibrin patch

To produce the fibrin patch, the Tissucol duo Baxter fibrin adhesive was used. Eight microliters of Tissucol solution was mixed with 1.5×10^6 transduced cells or culture medium. Then, 8 μL of thrombin solution was added for jelling. Fibrin patches loaded with cells were cultured in their corresponding medium, DMEM or EGM-2, for 24 h. Cell-loaded and nonloaded fibrin patches were then implanted after myocardial infarction induction using synthetic surgical glue (Glubran®2) in the healthy myocardium. After 3 weeks postimplantation, hearts were arrested in diastole with arrest solution [32], excised, fixed, cryopreserved in

30% sucrose in PBS, embedded in Tissue-Tek® Optimum Cutting Temperature™ (OCT™) compound (Sakura), and snapfrozen in liquid-nitrogen-cooled isopentane.

Noninvasive BLI of luciferase activity from implanted fibrin patches

For in vivo BLI, anesthetized mice bearing fibrin patches seeded with luciferase-reporter-expressing cells were intraperitoneally injected with 150 µL of luciferin (16.7 mg/mL in physiological serum; Caliper) to image PLuc activity. Alternatively, mice were intravenously tail-vein injected with 25 µL of benzyl coelenterazine (1 mg/mL in 50/50 propileneglycol/ethanol; Nanolight Technology) diluted in 125 µL of water to image *Renilla reniformis* luciferase (RLuc) activity. Imaging of PLuc and RLuc activities was performed in consecutive days. Mice were monitored during 3-week periods at the indicated times. Quantification and analysis of photons recorded in images was done using the Wasabi image analysis software (Hamamatsu Photonics).

Immunohistochemistry

Mouse heart cryosections were incubated with primary antibodies against CD31 (1:25; Abcam), cTnI (2 µg/mL; Abcam), or phospho-histone3 (phospho-H3) (2 µg/mL; Cell Signaling Technology). Sections were also incubated with antibodies against RFP and GFP (Abcam) to enhance detection of transduced cells. Secondary antibodies conjugated with Cy2, DyLight 549, and Cy5 (1 µg/mL; Jackson ImmunoResearch) were used for detection. Nuclei were counterstained with Hoechst 33342 and results were analyzed using a Leica TCS SP2 laser confocal microscope.

Vessel density

To determine vessel density at border and distal zones from the infarction, mouse heart sections were stained with biotinylated GSLI B4 isolectin (Vector Laboratories) and alexa fluor 647-conjugated streptavidin was used as a detection system. Images were taken in at least 10 randomly selected fields (five border areas + five distal areas) and analyzed using image analysis software (ImageJ; NIH). The results were expressed as percentage of mean isolectin-positive staining area per tissue surface.

Matrigel assay

hASCs and FP-ASCs were seeded in a 96-well plate precoated with 50 µL Matrigel™ (BD Biosciences) according to the manufacturer's instructions at a density of 10^4 cells/well in 100 mL EGM-2, six wells per patient, and culture condition was monitored every hour, during an 8-h period. Completely closed circle structures were quantified to evaluate vasculogenic capacity (circles/mm^2).

Statistical analysis

Statistical analysis was performed using a two-tailed Student's *t*-test. Values are presented as mean ± standard deviation. Descriptive statistics were performed with SPSS Statistics (15.0.1 version; SPSS, Inc.). Statistical tests were considered significant when $P < 0.05$.

Results

hASCs grown in EGM-2 display a fast-replicating phenotype

Generation of large numbers (typically 10^9–10^{10}) of cells for implantation is an important goal in the cell therapy field. Although hASCs have shown desirable properties for cell therapy, the time required for expansion, with the corresponding risk of genomic damage, is critical for some applications.

While evaluating procedures to optimize hASC expansion, it became apparent that exposure of hASCs to EGM-2 medium resulted in an FP-ASC with potential application in cell therapy.

hASCs from three different patients were grown in EGM-2 and DMEM (standard hASC growth media) as a control. As shown in Fig. 1A, during the exponential growth phase, duplication periods for EGM-2-grown hASCs (FP-ASCs) were on average 1.5 days, significantly shorter than those for

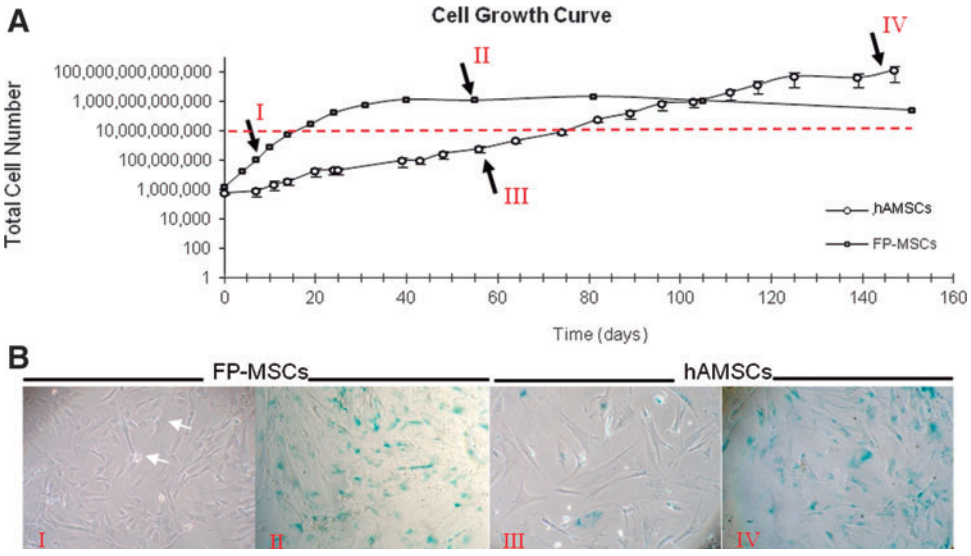

FIG. 1. Proliferation rate of hASCs is growth medium dependent. **(A)** The graph describes the proliferation capacity of hASCs in Dulbecco's modified Eagle's medium (DMEM) (*open symbols*) and in EGM-2 medium (*closed symbols*) [$n = 3$ for each condition; error bars, standard deviation (SD)]. The *red horizontal line* marks the 10^{10} cell level. Roman numerals (*arrows*) indicate the times at which β-galactosidase expression was assayed. **(B)** β-Galactosidase staining (*blue*), a senescence marker, shows entry of cells in the stationary growth phase. hASCs, human adipose-tissue-derived MSCs. Color images available online at www.liebertpub.com/scd

cells grown in DMEM, 5.1 days. Thus, average growth periods of 11.1 and 38.9 days were required to produce a total of 10^8 cells in each of these two media, respectively. Although FP-ASCs grew 3.5 times faster in EGM-2 than in DMEM, they reached the stationary phase earlier than those grown in DMEM. Moreover, regardless of their different replication rates, cells grown in EGM-2 and DMEM had similar maximum population doubling (PD) capacities, 19.5 and 24.4, respectively, following which, indications of cell senescence could be detected by β-galactosidase staining (Fig. 1B), indicative of their finite expansion capacity.

hASCs and FP-ASCs display equivalent multipotency and immunophenotypes

Since induction of a fast-replicating phenotype in hASCs by culture in EGM-2 medium could be accompanied by significant phenotypic changes, we analyzed hASC characteristics in FP-ASCs.

Conventional microscope observation indicated that FP-ASCs had MSC-like morphology, with slightly more pronounced spindle-like and fibroblastic appearance than native DMEM-grown hASCs. Multipotency was equivalent to that of hASCs and, under the appropriate conditions, FP-ASCs could be induced to differentiate to the osteogenic and adipogenic lineages (Fig. 2A).

We also compared the expression of CD34, CD13, CD29, CD44, CD90, CD105, CD73, and CD106 (MSC markers); CD49d and CD54 (specific hASC markers); CD31, VEGFR2, and CD144 (endothelial markers); and CD133 and c-Kit (stem cell markers) surface markers in early (average PD = 8.8) and late (average PD = 18.2) FP-ASCs, with those of the corresponding hASCs (average PD = 9.7) from three different patients (Supplementary Table S1; Supplementary Data are available online at www.liebertpub.com/scd).

Immunophenotyping results (Fig. 2B) showed an overall similarity in the surface marker expression pattern. However, there were significant differences ($^*P \le 0.05$; $^\dagger P \le 0.01$) in the proportion of cells expressing some of the markers, namely, CD49d, CD13, CD44, CD90, CD73, CD105, and CD133. In the case of CD105 and CD133, there were significant differences with early passage FP-ASCs. Except for CD106, CD133, and CD49d that were significantly more frequently expressed in FP-ASCs, the remaining ''significantly different'' makers were less-frequently expressed in FP-ASCs than in hASCs. In addition, the three MSC markers CD90, CD73, and CD105 were expressed in a lower proportion of the cells, and none of the endothelial markers were expressed.

FP-ASC safety

Due to the potential for therapeutic application of FP-ASCs, we assessed their oncologic safety. Exponential-growth (average PD = 8.8) and stationary-phase (average PD = 18.2) FP-ASCs, as well as the original hASCs (average PD = 9.7), from three different patients, were permanently transduced with a lentiviral vector for the expression of PLuc and implanted in the thigh muscle of SCID mice. Regular BLI monitoring of the cell-implanted mice showed that only a fraction of the implanted cells survive at the implantation sites, past day-25 postimplantation, and no indication of excessive cell proliferation or tumor

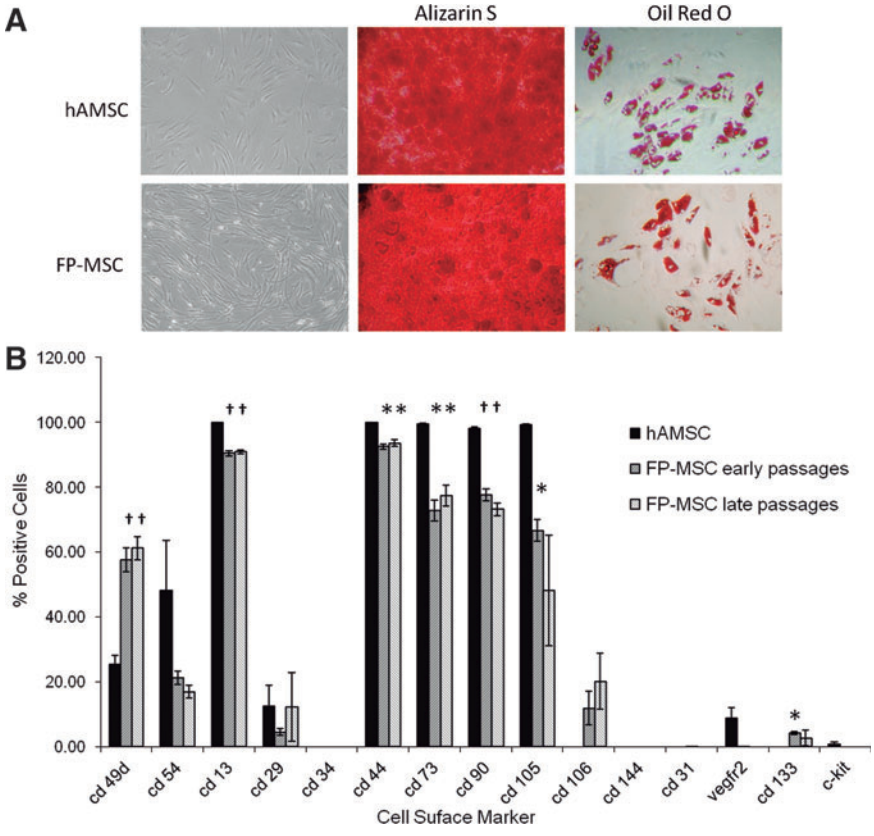

FIG. 2. hASCs and FP-ASCs display similar multipotency and immunophenotypes. **(A)** Panels show microphotographs of FP-ASC and hASC cultures, and their staining with alizarin S and oil red O, following induction to the osteogenic and adipogenic lineages, respectively. **(B)** The histogram compares the fraction of cells that express the indicated cell surface markers in hASCs (PD 10) from three different patients, with the corresponding early (PD 9) and late (PD 18) passage FP-ASCs. For analysis, CD markers were labeled using the corresponding fluorescence-conjugated antibodies and detected by FACS ($n = 3$, *t*-Student compared with hASCs for each marker: $^*P < 0.05$; $^\dagger P < 0.01$; error bars, SD). FP-ASCs, fast-proliferating phenotype; PD, population doubling. Color images available online at www.liebertpub.com/scd

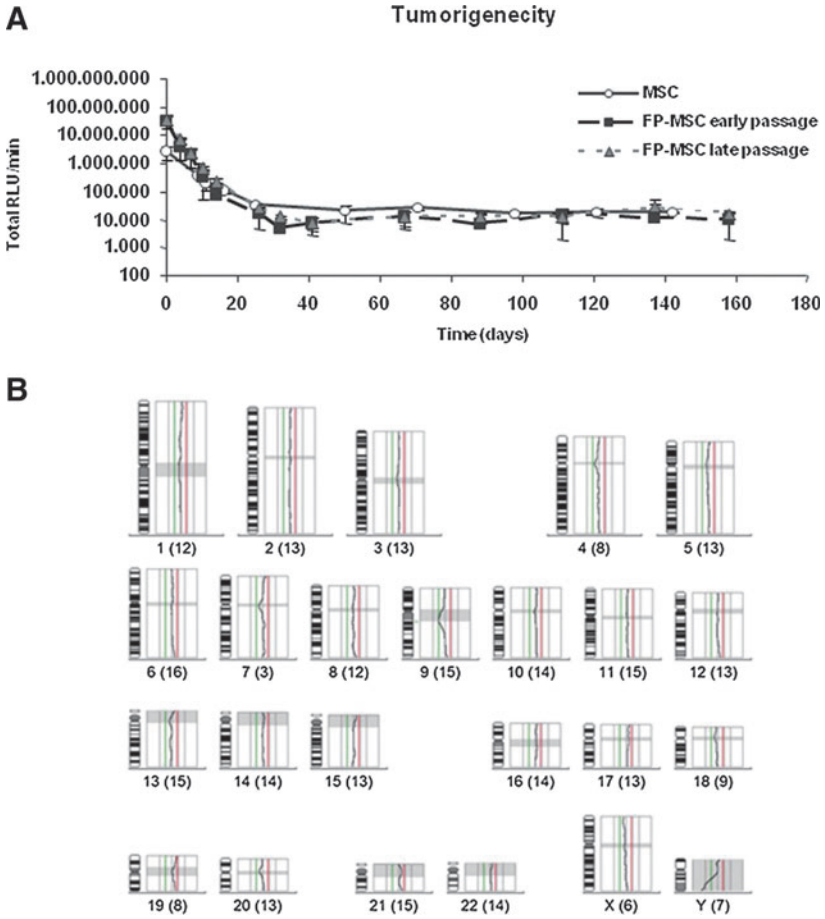

FIG. 3. Safety of FP-ASCs. Luciferase-expressing, early (PD 9) and late (PD 18), FP-ASCs were i.m. implanted in SCID mice and monitored regularly by BLI over a 160-day period. Normal hASCs (PD 10) were also implanted for comparison. **(A)** The graph represents the luciferase activity recorded from the BLI images of the implantation sites at the indicated days. Data points represent average values ± SD (*bars*) ($n = 6$ for each of the patient-derived cells). **(B)** Representative image showing a CGH profile from a late-passage FP-ASC patient sample. *Shaded areas* corresponding to centromeres and constitutive heterochromatin are not considered. The *vertical lines*, *left* and *right* of the CGH profile, represent fluorescence ratio limit values of 0.5–0.75 (*red*) and 1.0–1.25 (*green*). CGH ratio values between 1.25 and 0.75 indicate no significant gain or loss of cell DNA relative to control DNA and are considered normal. The actual ratio (*black line*) between test DNA and control DNA shows no gain or loss of DNA by the chromosomes. Numbers under each diagram indicate chromosome number and the number of chromosomes tested (*parenthesis*), respectively. SCID, severe-combined immunodeficient mouse; BLI, bioluminescent imaging; CGH, comparative genome hybridization. Color images available online at www.liebertpub.com/scd

generation was detected even after a 160-day period of regular monitoring (Fig. 3A).

Moreover, we also used CGH to evaluate genetic stability and detect possible gross genomic anomalies in exponentially growing (average PD = 8.8) and stationary (average PD = 18.2) FP-ASCs as well as in the original hASCs from the three patients (Fig. 3B).

In agreement with the animal studies, all of the samples ($n = 9$), except one that presented a 21 chromosome trisomy, had a normal karyotype and no genomic anomalies. Further revision of the trisomic patient showed that the trisomy was already pre-existent in the original hASCs, previous to expansion.

FP-ASCs display a characteristic gene expression pattern

To further characterize FP-ASCs we compared their gene expression patterns with those of their matching original hASCs.

mRNA from exponentially growing FP-ASCs and hASCs (average PD = 11.6 and 10.8, respectively) was analyzed using the Human Gene 1.0 ST array from Affymetrix, and interpreted with the Partek Genomics Suite (Partek, Inc.). The recovered *P*-values were then corrected using a step-up false discovery rate of 20% and the resulting list of significantly differently expressed genes was filtered to include only genes that demonstrated 1.5-fold, or larger, up- or downregulation in FP-ASCs relative to hASCs (Supplementary Fig. S1). Finally, to obtain further insight on potential biological processes involving the differentially expressed genes, we performed an Ingenuity Knowledge Base search using the IPA application.

The top-scoring networks identified were ''Cellular Growth and Proliferation, Cell Morphology, Cell Death'' (score 82) (Fig. S1A) and ''Cellular Movement, Cell-to-Cell Signalling and Interaction, Cellular Development'' (score 34) (Fig. S1B). In both the networks, upregulated FP-ASC genes predominate over the downregulated ones. From these two networks, a list of 12 genes was selected according to highest fold change (FC) and function annotation (''Cellular Growth and Proliferation'' *P*-value < 0.05 and/or ''Cellular Movement'' *P*-value < 0.05) (Fig. S1C) and then validated by RT-PCR in all the cell types and in an extra FP-ASC and hASC pair, as a control from an additionally different patient, patient 4. The FC values obtained by RT-PCR for this subset of genes expressed in FP-ASCs from the four patients, relative to the corresponding hASCs of origin, are summarized in Table 1 (columns 4–7), and compared using a *t*-Student paired test (Table 1, column 8; $^{*}P < 0.05$; $^{\dagger}P < 0.1$). RT-PCR values confirmed that all of the genes in the subset are upregulated in all FP-ASCs studied and for most of the genes the FC in expression are significant ($^{\dagger}P < 0.1$; $^{*}P < 0.05$). Thus, with this procedure we defined a gene expression profile induced in hASCs grown in EGM-2 that aids in the characterization of the FP-ASC phenotype.

TABLE 1. CHANGES IN GENE EXPRESSION OF FP-ASCS VERSUS hASCS

Genes	*Network*	*Function Anotation*	*Patient 1*	*Patient 2*	*Patient 3*	*Patient 4*	*Average FC (t-test paired)*	*Clone M05*	*Clone M17*	*Clone M27*	*FC clones (t-test patients vs clones)*
alox15b	2	migration of cells, proliferation of cells	2,156.4	1,683.7	1,269.1	566.8	**1,419.0** *	6,165.9	3,029.5	2,7163.3	**3,790.5** $P > 0,05$
ccl20	2	migration of cells, proliferation of cells	761.2	582.1	46.7	38.4	**357.1** n.s.	1,604.4	15.7	5.9	**542.0** $P > 0,05$
cnrl	1	migration of cells, proliferation of cells	375.2	38.8	334.5	168.3	**229.2** *	0.3	19.0	0.1	**6.5** $P > 0,05$
fkbp5	1	proliferation of cells	82.6	69.9	54.9	14.7	**55.5** *	4.2	130.0	18.6	**51.0** $P > 0,05$
hgf	1	migration of cells, proliferation of cells	186.8	19.7	20.8	20.0	**61.8** *	70.6	10.7	1.6	**27.6** $P > 0,05$
ptger2	1	migration of cells, proliferation of cells	105.8	798.2	101.2	807.7	**453.2** *	2.7	24.8	9.8	**12.4** $P > 0,05$
zbtb16	2	migration of cells, proliferation of cells	8,991.2	290.6	1,175.7	276.3	**2,683.4** *	1,804.8	2,040.0	408.5	**1,417.8** $P > 0,05$
areg/aregb	1	migration of cells, proliferation of cells	86.4	180.3	715.1	58.6	**260.1** †	464.1	173.0	301.7	**313.0** $P > 0,05$
cpm	2	proliferation of cells	176.2	121.3	147.3	37.8	**120.6** *	25.6	15.1	27.2	**22.6** $P > 0,05$
efnb2	1	migration of cells, proliferation of cells	70.7	73.4	966.3	24.9	**283.8** *	69.9	1,748.5	180.5	**666.3** $P > 0,05$
hsd11b	1	proliferation of cells	857.6	260.8	917.4	241.8	**569.4** †	1,312.5	457.9	357.4	**709.3** $P > 0,05$
maoa	2	migration of cells	631.8	192.1	675.9	62.3	**499.9** *	76.6	2.9	4.4	**28.0** $P > 0,05$

Averages (bold); *$P < 0.05$; †$P < 0.01$; FC, fold changes.

Induction of the FP-ASC phenotype

To verify that the FP-ASC phenotype is a reproducibly inducible trait of individual hASCs when grown in EGM-2, we devised the following subcloning strategy. hASCs from patient 4 were plated at 1 cell per well limiting dilution, in five 96-well plates in DMEM. Of these, ~6.7% of the wells (32 wells) generated single colonies from one cell. Following expansion in DMEM, single colonies were divided into two; one of which was maintained in DMEM and the other was changed to EGM-2 medium (FP-ASC conditions). Of all the colonies obtained, 30% were grown in both culture conditions and expanded for >15 PDs. Again, duplication time for the different clones in both media was significantly different [1.79 days in EGM-2 vs. 3.74 days in DMEM ($p < 1 \times 10^6$)] in agreement with previous data obtained from the different patients.

Total RNA extracted from three pairs of sister clones from each condition, which had reached 30,000 cells (~15 PD), was analyzed by RT-PCR for the expression of the 12 upregulated genes that characterize the FP-ASC phenotype. FC in gene expression for each FP-ASC–hASC pair of sister clones are summarized in Table 1 (columns 9–11).

A *t*-Student paired test comparison of the FC values for each of the 12 FP-ASC signature genes, from the group of three clones, with the FC values for the same genes from the four patients resulted in a $P > 0.05$ (Table 1, column 12). This result indicates that the difference in expression level of the signature genes between FP-ASCs and hASCs grown in the two conditions was not significative. In other words, whether we compared sister colonies grown in DMEM and EGM-2, or whole cell populations derived from the four different patients, also grown in DMEM and EGM-2, we obtained a similar pattern of changes in gene expression. This result shows that EGM-2 induces the observed FP-ASC phenotype in individual cell clones; thus, the FP-ASC phenotype is a general, EGM-2-inducible characteristic of hASCs.

FP-ASC phenotype reversibility

To determine whether the induction of the FP-ASC phenotype is a reversible process, we reversed the culture conditions of cells from patient 4 and clone M27. Thus, FP-ASCs were changed to DMEM and, conversely, hASCs were changed to EGM-2. Total RNA was extracted after 1 and 2 weeks in the new culture conditions, and analyzed by RT-PCR for expression of the 12 upregulated signature genes that characterize the FP-ASC phenotype (Supplementary Fig. S2A). FP-ASCs from patient 4 that were changed to DMEM lost their fast-proliferating phenotype and the FC of the analyzed genes fell drastically in just 1 week, with the expression levels of these 12 genes approaching those of hASCs grown in DMEM (Supplementary Fig. S2B). For clone M27 grown in EGM-2 (M27-E) the change to DMEM resulted in a reduction of its replication rate as well as in a reduction of the FC of the analyzed genes, as compared with the FC of the control clone, which was maintained in EGM-2. Although the expression level of the analyzed genes dropped over time, it did not reach the same baseline levels during the experiment (Supplementary Fig. S2B). Thus, FP-ASCs, a phenotype intimately linked to

growth in EGM-2 medium, are a reversible property of both, cell populations and individual clones.

Angiogenesis in vitro

The capacity of hASCs for endothelial lineage differentiation is well documented. We performed in vitro assays to compare the vasculogenic capacity of FP-ASCs and hASCs in Matrigel. Our results show (Fig. 4) that FP-ASCs are not only vasculogenic in this assay, but also generate significantly more abundant, better organized, and longer lasting vascular-like structures than those generated from hASCs.

Noninvasive BLI monitoring of FP-ASC and hASC differentiation to cardiac and endothelial lineages in a mouse model of myocardium infarct

To evaluate the potential of FP-ASCs for cell therapy, we used a mouse model of myocardium infarct in which we implanted FP-ASCs and hASCs expressing luciferase reporters, a strategy that allows in vivo monitoring of changes in the expression of specific genes. To do this, FP-ASCs and hASCs were each first labeled with a RLuc-RFP chimerical reporter regulated by the constitutively active cytomegalovirus promoter useful to evaluate cell number. Positively labeled cells expressing RFP were selected by FACS and labeled a second time with a different firefly luciferase-eGFP chimerical construct, this time regulated by either the inducible promoters of the PECAM-1 or the Troponin-I genes, as reporters of endothelial or cardiomyocytic lineage differentiation, respectively (PECAM-1p:Pluc:eGFP and hcTnPIp:Pluc:eGFP). The transduced cells were then seeded in a fibrin patch and implanted over the wound area of a myocardium infarct model in SCID mice. The proliferative and differentiation behavior of the implanted cells was noninvasively monitored by BLI during a 3-week period (Supplementary Fig. S3). Quantification of photon counts from both cell types showed a time-dependent increase in the ratio ''Pluc/Rluc,'' a magnitude that evaluates the proportion of light generated by the inducible promoter (PECAM-1 or Troponin-I)–regulated luciferase relative to that generated by the constitutively active CMV promoter. With this procedure potential artifacts due to changes in the number of light-emitting cells are taken into consideration.

The experiment results (Fig. 5A) indicate that, relative to the time of implantation, there were detectably increasing changes in the activity of the promoters regulating the expression of genes involved in the differentiation to cardiac and endothelial lineages for both FP-ASCs and hASCs. By the end of the experiment, there was a net increase in the activity of the PECAM-1 and Troponin-I promoters relative to week 0, although no significant difference could be detected between FP-ASCs and hASCs in

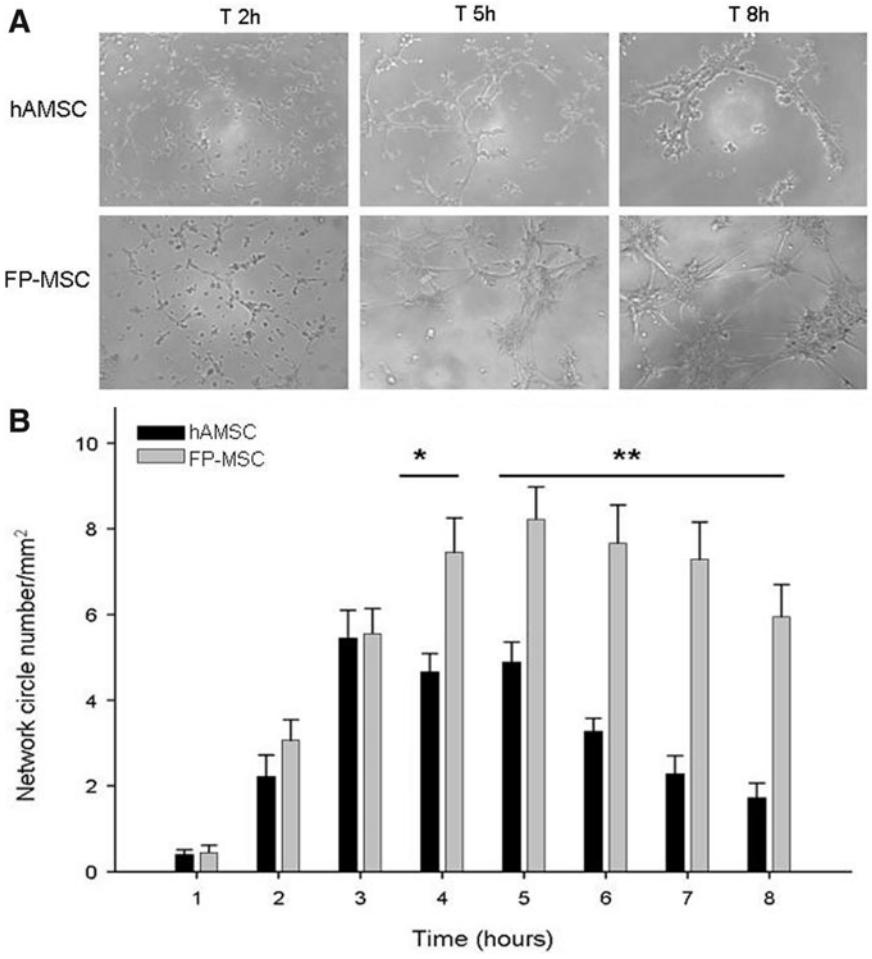

FIG. 4. Vascular capacity of hASCs and FP-ASCs. **(A)** Representative microphotographs showing tubular structures induced by Matrigel in cultures of hASCs and FP-ASCs, at the indicated times. **(B)** The histogram represents the quantification of Matrigel-induced tubular structures (circles/mm^2). Values for FP-ASCS and hASCs were compared using the *t*-Student test for each time point ($*P < 0.01$; $**P < 0.001$).

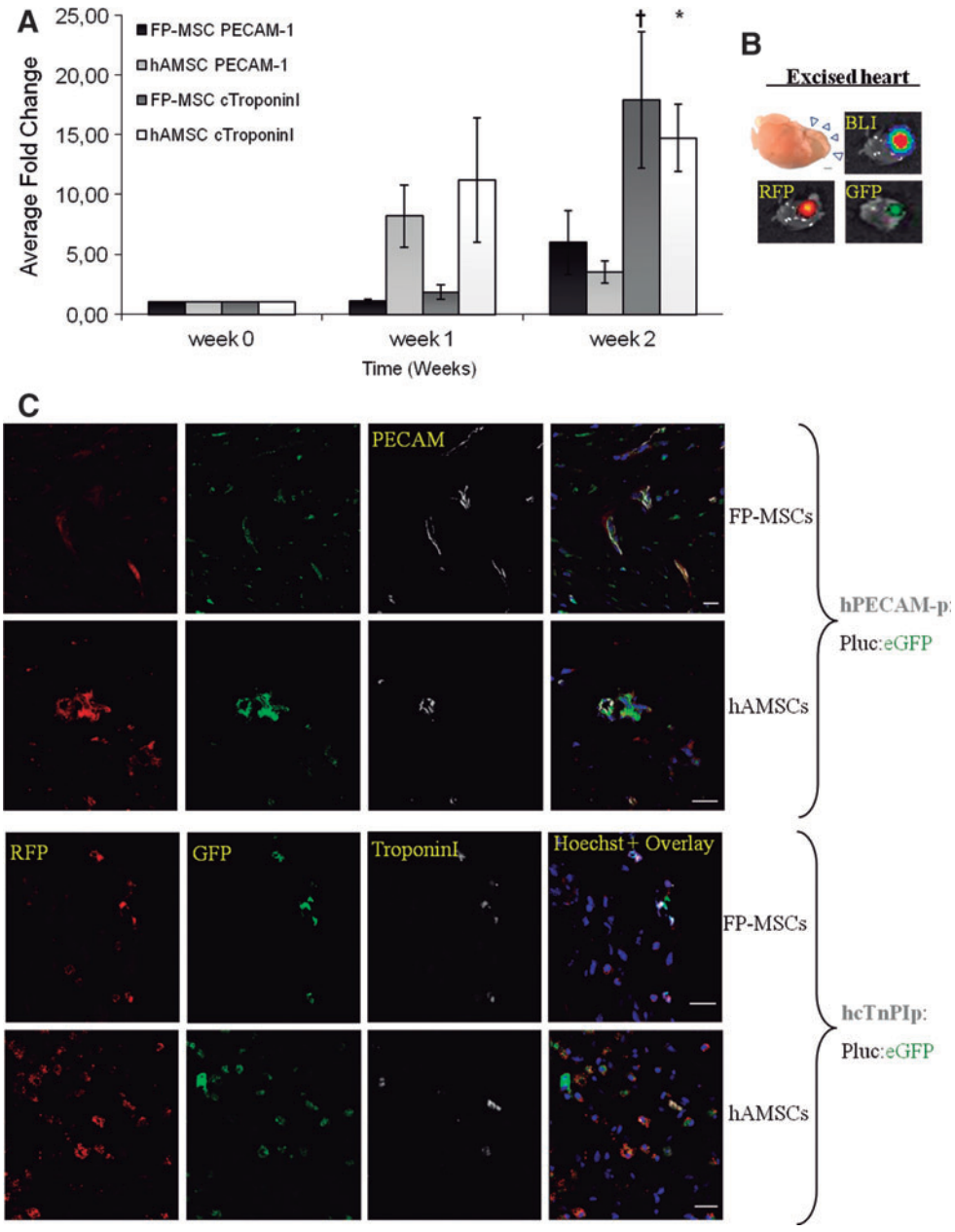

FIG. 5. In vivo differentiation capacity of heart-implanted hASCs and FP-ASCs. hASCs and FP-ASCs were doubly labeled with either Troponin-1 or PECAM-1 inducible promoter–regulated PLuc-EGFP, and constitutive CMV promoter–regulated RLuc-RFP constructs and seeded in a fibrin patch. The fibrin matrix was then implanted over the ventricular area of myocardium infarct model in mice and imaged by BLI regularly. The ratio of PLuc to RLuc photons (PLuc/RLuc), recorded in the BLI images, was used to evaluate the changes in inducible promoter activity. **(A)** The histogram represents the change in PLuc/RLuc ratio relative to implantation day (week 0) for each cell type and reporter, $n = 4$. **(B)** Heart excised after the BLI experiment showing epifluorescent and bioluminescent signals from stem cells seeded in the fibrin patch. **(C)** Fluorescence confocal microscope images of myocardial sections 3 weeks p.i. showing from *left* to *right*: RFP constitutively expressed in all the implanted hASCs and FP-ASCs; EGFP expressed in hASCs and FP-ASCs that differentiated to either the endothelial lineage (PECAM-1 promoter, *top panel*) or to the cardiomyocytic lineage (Troponin-I promoter, *bottom panel*); protein antigens, Troponin-I and PECAM-1, detected using the corresponding anti-Troponin-I and anti-PECAM-1 antibodies, shown in *gray* (*top* and *bottom panels,* respectively); overlay of the previous images plus Hoechst staining of nuclei. In each *panel*, the *top row* shows FP-ASCs while the *bottom row* shows hASCs. PLuc, *Photinus pyralis* luciferase; RLuc, *Renilla reniformis* luciferase. Color images available online at www.liebertpub.com/scd

either case. However, activity of the Troponin-I promoter was significantly higher than that of PECAM-1, in both hASCs and FP-ASCs, relative to W0 ($^{*}P < 0.05$, $^{\dagger}P < 0.1$). Although only the bioluminescence signal from the reporters could be detected noninvasively, we could easily identify the epifluorescent and bioluminescent signals of the implanted cells in the excised hearts (Fig. 5B).

Laser confocal microscopy was used to analyze tissue slices from the injury site, including the fibrin scaffold, 3 weeks p.i. In all cases, we were able to confirm the presence

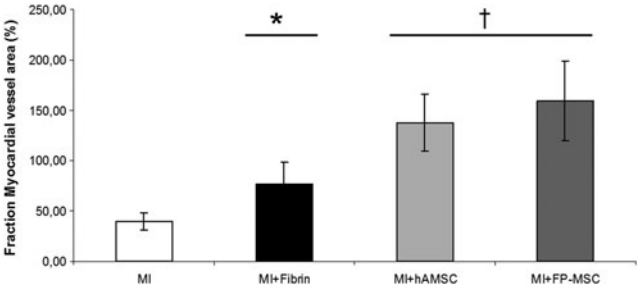

FIG. 6. Vasculogenic effect of therapeutic cells. The *histogram* shows the fraction (%) of myocardial-vessel area subjacent to the infarct in the MI model subjected to treatment with the fibrin patch, or the fibrin patch plus therapeutic cells. Vascular area was estimated using lectin staining. Values represent the average ± SD ($^*P < 0.05$; $^\dagger P < 0.005$, relative to the MI control).

of cells expressing RFP within the fibrin scaffold. However, only occasional red FP-ASCs were detected within the myocardium zone (data not shown). In the case of mice implanted with either FP-ASCs or hASCs labeled with the PECAM-1-regulated reporter, confocal microscope images revealed (Fig. 5C, top panel) the presence of red fluorescent cells that were also green fluorescent and expressed the PECAM-1 protein, as revealed by an antihuman PECAM-1-specific antibody (far-red fluorescent signal). In the case of mice implanted with either FP-ASCs or hASCs labeled with the Troponin-I-regulated reporters, confocal images revealed (Fig. 5C, bottom panel) the existence, within the fibrin patches, of frequent red fluorescent cells that were also green fluorescent and expressed the Troponin-I protein, as revealed using an antihuman Troponin-I-specific monoclonal antibody (far-red fluorescent signal). Thus, our results indicate that both FP-ASCs and hASCs are capable of differentiating to myocardial and endothelial phenotypes when implanted in fibrin scaffolds over the injured tissue, further supporting the in-vivo-generated BLI data.

Measurement of the fraction of vessel area in the myocardium adjacent to the infarct showed (Fig. 6) that while treatment with fibrin alone resulted in an improvement in vascularization (76.4% vs. 40.1% in control group, $^*P < 0.05$), the inclusion of hASCs or FP-ASCs in the fibrin patch had an even more profound and significant vascular-inducing effect (137.7% and 159.1%, respectively, $^\dagger P < 0.005$), been FP-ASCs the most effective cell type.

Discussion

Cell therapy using stem cells is a promising therapeutic strategy for many conditions requiring tissue replacement, in particular, when there is a scarcity of organs for transplantation or the danger of contamination by foreign organisms.

An important hurdle for cell therapy is the requirement for large numbers of cells; clinical treatments frequently require more than 1.5×10^8 therapeutic cells (2×10^6/kg × 75 kg). The expansion time required for procurement of sufficient cells is strongly dependent on the initial number of cells available and, when this is low, extended culture times are required. Since the ex-vivo-expansion rate is not only limited, but also decreases over time, long propagation times may result in accumulation of genetic damage and loss of multipotentiality, together with phenotypic and functional changes related to cell senescence. Nevertheless, reports on the likelihood of oncologic transformation have not been substantiated [33,34] and no tumors have been reported after transplant of MSCs without and with genetic defects during 8 weeks (mice) and 2 years (allogeneic, human) [35], respectively.

The growth of hASCs in EGM-2, an endothelial cell medium, which also promotes endothelial differentiation, was previously described by Yoshimura's lab in 2007 [36], and it has also been used with other cell types, such as dendritic cells [37] or smooth muscle progenitor cells [38,39].

In the current work, we analyze changes taking place in hASCs grown in EGM-2 medium that lead to a phenotype that while preserving a developmental potential equivalent to that of DMEM-grown hASCs is endowed with the advantage of been fast-proliferating, self–limiting, and safe, thus, providing a potentially useful resource of cells for therapy.

We show that hASCs grown in EGM-2 medium, referred to as FP-ASCs, suffer fibroblastic-like morphologic changes and proliferate up to 3.5 times faster than hASCs grown in standard DMEM. This latter feature allows the generation of 10^{10} cells in close to 3 weeks, while it took others ~75 days to achieve the same number of cells, a prohibitive delay, for some therapeutic applications.

The contribution of growth factors in EGM-2 to ASC proliferation has been the subject of previous research. Some studies have shown increases in the proliferation rate of hASCs grown in defined SF/SX media StemPro (Gibco); however, these tended to be lower than those in EGM-2 reported here [13,40]. The effects of growth factors insulin growth factor (IGF)-1, epidermal growth factor (EGF), and vascular endothelial growth factor (VEGF) on cell proliferation have been explored by several authors and found to have some, but not significant, cell-proliferation-promoting capacity when tested individually [20–22], although others [41] report that prolonged exposure of hASCs to EGF results in a significant increase in cell proliferation and inhibition of adipose differentiation. It has also been reported that PDGF and EGF may have a reducing effect in cell proliferation and adipogenic differentiation [20]. Only FGF-2 by itself has shown a statistically significant capacity to promote cell growth [19,20,23,24]. However, the effect of FGF-2 was not enough to explain the cell-proliferation-promoting effects of EGM-2. Thus, it would appear that the capacity of EGM-2 to induce cell proliferation seems to result from a synergistic effect of growth factors, including those in FBS.

March and coworkers [42] describe the production of hepatocyte growth factor (HGF), VEGF, granulocyte-macrophage colony stimulating factor (GM-CSF), transforming growth factor-beta (TGF-β), and FGF-2 by hASCs grown in EBM-2. Interestingly, VEGF, TGF-β, and FGF-2 are also constituents of the growth factor supplement added to defined media EBM-2 to produce EGM-2; IGF is likely provided by FBS. These results suggest that hASC-secreted growth factors may have autocrine roles regulating endothelial differentiation, proliferation, and survival in this defined media. Our microarray analysis results show that only HGF is overexpressed in FP-ASCs relative to hASCs, while VEGF, GM-CSF, and TGF-β are expressed at the same level.

FP-ASCs and hASCs share the majority of surface markers, and equivalent (osteogenic and adipogenic) in vitro differentiation potential. However, we also found some significant

differences between both cell types. FP-ASCs maintained the expression pattern of markers that define the MSCs ($CD105^+$, $CD73^+$ y $CD90^+$, and $CD34^-$) but in a significantly lower fraction of the cells. $CD105^-$ subpopulation cells could have some protherapeutic properties, promoting differentiation and regulating T cells [43]. Among other differences, CD106 (Vascular cell adhesion molecule), absent in hASCs, and CD49d (Very-late antigen 4) that interact with each other play roles in stabilizing lymphocyte adhesion to endothelial cells and stimulation of T cells [44] and are more often expressed in FP-ASCs. However, FP-ASCs did not express any of CD31, VEGFR2, and CD144, characteristic endothelial lineage markers that were analyzed.

Our assays indicated that FP-ASCs are safe. While replicating faster than hASCs, the total proliferation potential of FP-ASCs was similar to that of hASCs, and both cell types entered senescence, considered a safeguard against neoplasic transformation [45], after a similar number of replication rounds. By CGH tests, we were able to show that no gross chromosomal anomalies could be found in FP-ASCs grown in EGM-2 after 9 and 18 PDs (exponential and stationary growth phases, respectively). Moreover, in vivo BLI imaging studies showed that following implantation in mice, cells were also functionally safe and no excessive cell proliferation or tumor generation was detectable even after a 160-day period of regular monitoring.

Growth in EGM-2 induced in FP-ASCs a characteristic pattern of changes in gene expression. According to the analysis of gene expression array results by an Ingenuity Knowledge Base search using the IPA application, FP-ASCs overexpressed genes associated with ''Cellular Growth and Proliferation, Cell Morphology, Cell Death'' (score 82) and ''Cellular Movement, Cell-to-Cell Signalling and Interaction, Cellular Development'' (score 34). Based on this analysis we selected a list of 12 genes with the highest FC, functionally annotated as ''Cellular Growth and Proliferation'' ($P < 0.05$) and/or ''Cellular Movement'' ($P < 0.05$). This gene set was validated using RT-PCR and used to characterize FP-ASCs.

The FP-ASC phenotype is robust, and can be reproducibly induced in both, the general hASC population from patients with different genetic backgrounds, and in clones derived from single hASCs. Using the 12-gene-list expression pattern described as an FP-ASC profile, we showed that hASC clones derived from a single cell could be induced by EGM-2 to a phenotype not significantly different than that induced by EGM-2 in the general hASCs population, and that such FP-ASC clones had an average duplication rate (1.79 days) significantly shorter than that of sister cells in DMEM (3.74 days). Moreover, reversing culture conditions, for growth in DMEM, resulted also in the reversal to the hASC-like expression phenotype and slower growth rate.

As shown by previous reports [46] and also our current results, cell growth conditions during expansion in culture and storage can significantly affect growth rate, gene expression, senescence, and differentiation capacity and can ultimately impact on therapeutic efficacy. Thus, in support of a recent FDA perspective on MSC product characterization for clinical trials [47], gene expression profiles, in particular those relative to cell surface markers, growth factors, and cytokines could be valuable parameters to consider when evaluating the potential hASCs and derivatives generated under a variety of conditions for clinical applications.

Marchal et al. [25] have provided credible data in support of an endothelial-like cell type [multipotent endothelial-like cells (ME-LC)] with endothelial and cardiomyocytic differentiation potential that can be selected from hASC populations through an elaborate process including growth in EGM-2. However, while ME-LC and FP-ASC types share endothelial and cardiomyocyte differentiation potential and express common endothelial hematopoietic marker VEGFR (KDR) and EPC marker CD133, contrary to ME-LCs, FP-ASCs do not express CD34 or CD45. There are other important differences between both cell types. While ME-LC production requires lengthy (2 months) process, the FP-ASC phenotype is easily produced by change of growth medium from DMEM to EGM-2. Moreover, we also show that cloned hASCs can be induced to the FP-ASC phenotype, cloned again, and induced back to the ASC phenotype. Thus, FP-ASCs do not derive, as claimed for ME-LCs, from endothelial-like precursor preexistent in the hASC population, but they result from growth factor induction of hASCs.

FP-ASCs could have angiogenesis-related therapeutic applications. FP-ASCs were more effective at inducing the formation of larger and longer-lasting vascular structures in in vitro matrigel assays than hASCs. Moreover, FP-ASCs had also a more potent angiogenic-inducing effect when implanted in a fibrin patch over an MI injury model in mice. Since implanted cells were limited to the fibrin scaffolds, not migrating to adjacent myocardium, a likely explanation of these results could be the paracrine effects of differential expression of molecules related to secretion of growth factors and cytokines [5]. From our gene expression analysis we find that several growth factors—AREG/AREGB, HGF, and GDF5 (growth differentiation factor 5)—and cytokines—Tnfsf4, CXCL5, CCL20, CMTM8, and NAMPT—are significantly upregulated in FP-ASCs relative to ASCs, while INHBA, NGF, NOV, and NTF3 are downregulated relative to ASCs in support of the concept of ASCs as growth factor factories.

In vivo BLI monitoring of bioluminescent FP-ASCs and hASCs implanted in a mouse MI model using the fibrin scaffold showed that FP-ASCs and hASCs had a similar capacity to differentiate to the endothelial lineage. However, FP-ASCs were more effective at myocardial differentiation. These results were validated by histological analysis that demonstrated the presence of red fluorescent cells also expressing green fluorescent protein as a result of PECAM-1 or Troponin-I promoter activation, and the corresponding PECAM-1 and Troponin-1 proteins, revealed by the specific antibodies.

Conclusions

Growth of hASCs in EGM-2 medium induces a fast-proliferating phenotype (FP-ASCs) that reduces by a factor of 3.5 the time required to produce sufficient cells for therapy; it is genetically stable, generates no tumors in mice, and has differentiation potential equivalent to that of hASCs.

The FP-ASC phenotype is a reversible phenomenon that can be characterized by changes in the expression of 12 different genes.

Gene expression profiling could be a useful tool to evaluate therapeutic potential of hASCs for clinical trials.

FP-ASCs generate larger and more stable vascular structures in Matrigel, are better paracrine inducers of angiogenesis, and differentiate better to the cardiomyogenic lineage than hASCs in a live animal model.

Due to the ease with which FP-ASCs can be generated, these cells could be a promising resource for therapy.

Acknowledgments

This work was funded by grants from the Ministerio de Economía y Competitividad SAF2009-07102, and Red Temática de Investigación Cooperativa TerCel, ISCiii (RD12/0019/0029). The authors specially thank Dr. Josep Roca, from ''System Roca'' (Centro Medico Delfos), for the kind donation of liposuction samples for hASC preparation.

Author Disclosure Statement

The authors declare no conflicts of interest.

References

1. Bernardo ME, D Pagliara and F Locatelli. (2012). Mesenchymal stromal cell therapy: a revolution in regenerative medicine? Bone Marrow Transplant 47:164–171.
2. Lin CS, ZC Xin, CH Deng, H Ning, G Lin and TF Lue. (2010). Defining adipose tissue-derived stem cells in tissue and in culture. Histol Histopathol 25:807–815.
3. Lin G, M Garcia, H Ning, L Banie, YL Guo, TF Lue and CS Lin. (2008). Defining stem and progenitor cells within adipose tissue. Stem Cells Dev 17:1053–1063.
4. Kern S, H Eichler, J Stoeve, H Kluter and K Bieback. (2006). Comparative analysis of mesenchymal stem cells from bone marrow, umbilical cord blood, or adipose tissue. Stem Cells 24:1294–1301.
5. Nakanishi C, N Nagaya, S Ohnishi, K Yamahara, S Takabatake, T Konno, K Hayashi, MA Kawashiri, T Tsubokawa and M Yamagishi. (2011). Gene and protein expression analysis of mesenchymal stem cells derived from rat adipose tissue and bone marrow. Circ J 75:2260–2268.
6. Chandra V, G Swetha, S Phadnis, PD Nair and RR Bhonde. (2009). Generation of pancreatic hormone-expressing islet-like cell aggregates from murine adipose tissue-derived stem cells. Stem Cells 27:1941–1953.
7. Constantin G, S Marconi, B Rossi, S Angiari, L Calderan, E Anghileri, B Gini, SD Bach, M Martinello, et al. (2009). Adipose-derived mesenchymal stem cells ameliorate chronic experimental autoimmune encephalomyelitis. Stem Cells 27:2624–2635.
8. Rasmussen JG, O Frobert, C Holst-Hansen, J Kastrup, U Baandrup, V Zachar, T Fink and U Simonsen. (2012). Comparison of human adipose-derived stem cells and bone marrow-derived stem cells in a myocardial infarction model. Cell Transplant 23:195–206.
9. Izadpanah R, C Trygg, B Patel, C Kriedt, J Dufour, JM Gimble and BA Bunnell. (2006). Biologic properties of mesenchymal stem cells derived from bone marrow and adipose tissue. J Cell Biochem 99:1285–1297.
10. Lazarus HM, ON Koc, SM Devine, P Curtin, RT Maziarz, HK Holland, EJ Shpall, P McCarthy, K Atkinson, et al. (2005). Cotransplantation of HLA-identical sibling culture-expanded mesenchymal stem cells and hematopoietic stem cells in hematologic malignancy patients. Biol Blood Marrow Transplant 11:389–398.
11. Ringden O, M Uzunel, I Rasmusson, M Remberger, B Sundberg, H Lonnies, HU Marschall, A Dlugosz, A Szakos, et al. (2006). Mesenchymal stem cells for treatment of therapy-resistant graft-versus-host disease. Transplantation 81:1390–1397.
12. Crapnell K, R Blaesius, A Hastings, DP Lennon, AI Caplan and SP Bruder. (2013). Growth, differentiation capacity, and function of mesenchymal stem cells expanded in serum-free medium developed via combinatorial screening. Exp Cell Res 319:1409–1418.
13. Patrikoski M, M Juntunen, S Boucher, A Campbell, MC Vemuri, B Mannerstrom and S Miettinen. (2013). Development of fully defined xeno-free culture system for the preparation and propagation of cell therapy-compliant human adipose stem cells. Stem Cell Res Ther 4:27.
14. Chieregato K, S Castegnaro, D Madeo, G Astori, M Pegoraro and F Rodeghiero. (2011). Epidermal growth factor, basic fibroblast growth factor and platelet-derived growth factor-bb can substitute for fetal bovine serum and compete with human platelet-rich plasma in the ex vivo expansion of mesenchymal stromal cells derived from adipose tissue. Cytotherapy 13:933–943.
15. Fekete N, MT Rojewski, R Lotfi and H Schrezenmeier. (2014). Essential components for ex vivo proliferation of mesenchymal stromal cells. Tissue Eng Part C Methods 20:129–139.
16. Gharibi B and FJ Hughes. (2012). Effects of medium supplements on proliferation, differentiation potential, and in vitro expansion of mesenchymal stem cells. Stem Cells Transl Med 1:771–782.
17. Schallmoser K, E Rohde, A Reinisch, C Bartmann, D Thaler, C Drexler, AC Obenauf, G Lanzer, W Linkesch and D Strunk. (2008). Rapid large-scale expansion of functional mesenchymal stem cells from unmanipulated bone marrow without animal serum. Tissue Eng Part C Methods 14:185–196.
18. Seo JP, N Tsuzuki, S Haneda, K Yamada, H Furuoka, Y Tabata and N Sasaki. (2013). Comparison of allogeneic platelet lysate and fetal bovine serum for in vitro expansion of equine bone marrow-derived mesenchymal stem cells. Res Vet Sci 95:693–698.
19. Chiou M, Y Xu and MT Longaker. (2006). Mitogenic and chondrogenic effects of fibroblast growth factor-2 in adipose-derived mesenchymal cells. Biochem Biophys Res Commun 343:644–652.
20. Koellensperger E, D von Heimburg, M Markowicz and N Pallua. (2006). Human serum from platelet-poor plasma for the culture of primary human preadipocytes. Stem Cells 24:1218–1225.
21. Kras KM, DB Hausman and RJ Martin. (2000). Tumor necrosis factor-alpha stimulates cell proliferation in adipose tissue-derived stromal-vascular cell culture: promotion of adipose tissue expansion by paracrine growth factors. Obes Res 8:186–193.
22. Miranville A, C Heeschen, C Sengenes, CA Curat, R Busse and A Bouloumie. (2004). Improvement of postnatal neovascularization by human adipose tissue-derived stem cells. Circulation 110:349–355.
23. Quarto N and MT Longaker. (2006). FGF-2 inhibits osteogenesis in mouse adipose tissue-derived stromal cells and sustains their proliferative and osteogenic potential state. Tissue Eng 12:1405–1418.

24. Zaragosi LE, G Ailhaud and C Dani. (2006). Autocrine fibroblast growth factor 2 signaling is critical for self-renewal of human multipotent adipose-derived stem cells. Stem Cells 24:2412–2419.
25. Marchal JA, M Picon, M Peran, C Bueno, M Jimenez-Navarro, E Carrillo, H Boulaiz, N Rodriguez, P Alvarez, et al. (2012). Purification and long-term expansion of multipotent endothelial-like cells with potential cardiovascular regeneration. Stem Cells Dev 21:562–574.
26. Vilalta M, IR Degano, J Bago, E Aguilar, SS Gambhir, N Rubio and J Blanco. (2009). Human adipose tissue-derived mesenchymal stromal cells as vehicles for tumor bystander effect: a model based on bioluminescence imaging. Gene Ther 16:547–557.
27. Sanz L, P Santos-Valle, V Alonso-Camino, C Salas, A Serrano, JL Vicario, AM Cuesta, M Compte, D Sanchez-Martin and L Alvarez-Vallina. (2008). Long-term in vivo imaging of human angiogenesis: critical role of bone marrow-derived mesenchymal stem cells for the generation of durable blood vessels. Microvasc Res 75:308–314.
28. Rigola MA, C Fuster, C Casadevall, M Bernues, MR Caballin, A Gelabert, J Egozcue and R Miro. (2001). Comparative genomic hybridization analysis of transitional cell carcinomas of the renal pelvis. Cancer Genet Cytogenet 127:59–63.
29. Irizarry RA, BM Bolstad, F Collin, LM Cope, B Hobbs and TP Speed. (2003). Summaries of Affymetrix GeneChip probe level data. Nucleic Acids Res 31:e15.
30. Bago JR, E Aguilar, M Alieva, C Soler-Botija, OF Vila, S Claros, JA Andrades, J Becerra, N Rubio and J Blanco. (2013). In vivo bioluminescence imaging of cell differentiation in biomaterials: a platform for scaffold development. Tissue Eng Part A 19:593–603.
31. Bago JR, C Soler-Botija, L Casani, E Aguilar, M Alieva, N Rubio, A Bayes-Genis and J Blanco. (2013). Bioluminescence imaging of cardiomyogenic and vascular differentiation of cardiac and subcutaneous adipose tissue-derived progenitor cells in fibrin patches in a myocardium infarct model. Int J Cardiol 169:288–295.
32. Bayes-Genis A, C Soler-Botija, J Farre, P Sepulveda, A Raya, S Roura, C Prat-Vidal, C Galvez-Monton, JA Montero, D Buscher and JC Izpisua Belmonte. (2010). Human progenitor cells derived from cardiac adipose tissue ameliorate myocardial infarction in rodents. J Mol Cell Cardiol 49:771–780.
33. de la Fuente R, A Bernad, J Garcia-Castro, MC Martin and JC Cigudosa. (2010). Retraction: spontaneous human adult stem cell transformation. Cancer Res 70:6682.
34. Rubio D, J Garcia-Castro, MC Martin, R de la Fuente, JC Cigudosa, AC Lloyd and A Bernad. (2005). Spontaneous human adult stem cell transformation. Cancer Res 65:3035–3039.
35. Tarte K, J Gaillard, JJ Lataillade, L Fouillard, M Becker, H Mossafa, A Tchirkov, H Rouard, C Henry, et al. (2010). Clinical-grade production of human mesenchymal stromal cells: occurrence of aneuploidy without transformation. Blood 115:1549–1553.
36. Suga H, T Shigeura, D Matsumoto, K Inoue, H Kato, N Aoi, S Murase, K Sato, K Gonda, I Koshima and K Yoshimura. (2007). Rapid expansion of human adipose-derived stromal cells preserving multipotency. Cytotherapy 9:738–745.
37. Sprague L, M Muccioli, M Pate, E Meles, J McGinty, H Nandigam, AK Venkatesh, MY Gu, K Mansfield, et al. (2011). The interplay between surfaces and soluble factors define the immunologic and angiogenic properties of myeloid dendritic cells. BMC Immunol 12:35.
38. Simper D, PG Stalboerger, CJ Panetta, S Wang and NM Caplice. (2002). Smooth muscle progenitor cells in human blood. Circulation 106:1199–1204.
39. Xie SZ, NT Fang, S Liu, P Zhou, Y Zhang, SM Wang, HY Gao and LF Pan. (2008). Differentiation of smooth muscle progenitor cells in peripheral blood and its application in tissue engineered blood vessels. J Zhejiang Univ Sci B 9:923–930.
40. Yang S, L Pilgaard, LG Chase, S Boucher, MC Vemuri, T Fink and V Zachar. (2012). Defined xenogeneic-free and hypoxic environment provides superior conditions for long-term expansion of human adipose-derived stem cells. Tissue Eng Part C Methods 18:593–602.
41. Hauner H, K Rohrig and T Petruschke. (1995). Effects of epidermal growth factor (EGF), platelet-derived growth factor (PDGF) and fibroblast growth factor (FGF) on human adipocyte development and function. Eur J Clin Invest 25: 90–96.
42. Rehman J, D Traktuev, J Li, S Merfeld-Clauss, CJ Temm-Grove, JE Bovenkerk, CL Pell, BH Johnstone, RV Considine and KL March. (2004). Secretion of angiogenic and antiapoptotic factors by human adipose stromal cells. Circulation 109:1292–1298.
43. Anderson P, AB Carrillo-Galvez, A Garcia-Perez, M Cobo and F Martin. (2013). CD105 (endoglin)-negative murine mesenchymal stromal cells define a new multipotent subpopulation with distinct differentiation and immunomodulatory capacities. PLoS One 8:e76979.
44. Elices MJ, L Osborn, Y Takada, C Crouse, S Luhowskyj, ME Hemler and RR Lobb. (1990). VCAM-1 on activated endothelium interacts with the leukocyte integrin VLA-4 at a site distinct from the VLA-4/fibronectin binding site. Cell 60:577–584.
45. Ohtani N, DJ Mann and E Hara. (2009). Cellular senescence: its role in tumor suppression and aging. Cancer Sci 100:792–797.
46. Bellayr IH, JG Catalano, S Lababidi, AX Yang, JL Lo Surdo, SR Bauer and RK Puri. (2014). Gene markers of cellular aging in human multipotent stromal cells in culture. Stem Cell Res Ther 5:59.
47. Mendicino M, AM Bailey, K Wonnacott, RK Puri and SR Bauer. (2014). MSC-based product characterization for clinical trials: an FDA perspective. Cell Stem Cell 14: 141–145.

Address correspondence to:
Dr. Jeronimo Blanco
Cell Therapy Group
Institute for Advanced Chemistry of Catalonia (IQAC)
CSIC
c/Jordi Girona, 18-26
Barcelona 08034
Spain

E-mail: jeronimo.blanco@iqac.csic.es

Received for publication May 8, 2014
Accepted after revision July 3, 2014
Prepublished on Liebert Instant Online July 14, 2014